

Vulnerabilities of quantum key distribution systems in visible range

Boris Nasedkin,^{1,2,*} Azat Ismagilov,¹ Vladimir Chistiakov,² Andrei Gaidash,^{1,3} Aleksandr Shimko,⁴ Alexei D. Kiselev,¹ Anton Tsyarkin,¹ Vladimir Egorov,² and Anton Kozubov^{1,3}

¹Laboratory of Quantum Processes and Measurements, ITMO University,
199034, 3b Kadetskaya Line, Saint Petersburg, Russia

²Laboratory for Quantum Communications, ITMO University,
199034, 3b Kadetskaya Line, Saint Petersburg, Russia

³Department of Mathematical Methods for Quantum Technologies,
Steklov Mathematical Institute of Russian Academy of Sciences, 119991, 8 Gubkina St, Moscow, Russia

⁴Center for Optical and Laser materials research, Saint-Petersburg State University,
198504, 5 Ulianovskaya, Saint Petersburg, Russia

(Dated: August 15, 2024)

Spectral loopholes in the 1000-2100 nm range have been the focus of attention of quantum hacking research aimed at searching and elimination of vulnerabilities in quantum key distribution systems. In this work, we concentrate on shorter wavelengths ranged from 400 nm up to 800 nm and experimentally study spectra of insertion losses for a number of fiber optical components to assess potentials for their implementation as countermeasures. We show that efficiency of the elements commonly used as countermeasures against hacking attacks in the telecom range can be significantly impaired in the visible range. It is found that the vulnerabilities detected in this range play an increasingly important role for hacking strategies such as the induced-photorefractive attack, whose efficiency improves when the wavelength decreases. We consider security issues emerged due to the latter effect and discuss possible countermeasures if any for various utilization cases of phase-modulators.

I. INTRODUCTION

The security of quantum key distribution (QKD) systems hinges upon the fundamental laws of physics. Over the past decades, significant progress has been made in theoretical security proofs [1–12]. However, many of these proofs rest on the assumption of perfect and trusted devices. Such trust assumption imposes a rather strong security requirement, which is generally difficult to implement in practice. In real situations, imperfect devices in QKD systems would introduce vulnerabilities that can be exploited by eavesdroppers to extract additional information about the transmitted bits during their attacks as it is considered in [11–16]. Device-independent (DI) [17–21] and semi-device-independent [22–25] protocols have emerged as a prominent area of research that provides a way to prevent side-channel attacks [26]. On the opposite side, another rapidly developing field which is often referred to as quantum hacking has received a considerable amount of attention [27].

Emerging approaches in quantum hacking pose novel challenges for security analysis of QKD systems. Numerous vulnerabilities have been identified in prior works [28–30], underscoring the importance of enhancing security measures. Eavesdropper strategies in quantum hacking can broadly be classified under two basic types, active and passive, as well as combinations thereof. Active strategies involve the manipulation of optical parameters within the hardware, whereas passive strategies solely facilitate the acquisition of additional information.

A quintessential illustration of a passive attack is the Trojan-horse attack, which is also known as the large pulse attack [31, 32]. In this scenario, the eavesdropper (Eve) employs scanning pulses introduced into the systems of legitimate users (Alice and Bob) via the quantum channel, allowing for the extraction of distributed sequences from the reflected portions of the eavesdropper pulses back into the quantum channel. The key factors that determine the efficiency of this attack involve the transmittance of elements in two directions, the distinguishability of states along with countermeasures utilized in the system. An important point is that all these factors require the eavesdropper to define the optimal spectral range of wavelengths employed to perform attack.

The well-known detector blinding attack (DBA) [33–35] exemplifies an active attack. The idea underlying the attack is that, under the action of high-power laser radiation (as compared to typical intensities used in QKD), the operating mode of single photon detectors (SPDs) based on avalanche photodiodes can be changed from the Geiger mode into the linear operating mode, so that the eavesdropper can manipulate the clicks registered by the SPDs. The efficiency of this DBA based quantum hacking approach crucially depends on the spectral sensitivity of the avalanche photodiode, the transmittance of optical elements connecting the quantum channel with the single photon avalanche diode (SPAD), and the countermeasures implemented into the QKD system. So, it turned out that, similar to the Trojan-horse attack, the spectral range is one of the factors that govern the success of the DBA attack.

Previous studies [36–39] motivated by the THA, have mainly been focused on transmittance of fiber optical ele-

* banasedkin@itmo.ru

ments utilized in QKD systems at wavelengths ranged between 1000 nm and 2100 nm. For the 600-1000 nm range, the experimental results were reported in Refs. [39, 40].

But, for the above discussed DBA and the laser damage attacks (LDA) that exploit temperature dependence of the transmittance of fiber-optical elements [41–43], shorter wavelengths may also be used. At shorter wavelengths, low insertion losses of elements employed for countermeasures may lead to unnoticed and thus potentially successful delivery of radiation injected by Eve to the elements under attack.

New vulnerabilities at different wavelengths have been the subject of intense recent studies [44]. The induced-photorefractive attack (IPA) [27, 45] represent attacks that will do better in the visible spectral range [46]. In addition, this attack is claimed to be applicable for hacking measurement device independent (MDI) QKD systems [27].

The main targets of the IPA are phase and amplitude modulators based on photo-refractive crystals, where variations in refractive index or transmittance can be induced by light. The IPA strategy enables Eve to manipulate the characteristics of quantum states, i.e. mean photon number, at the sender’s side using laser radiation. The efficiency of these attacks improves as the radiation wavelength becomes shorter [46]. So, it is important to perform spectral measurements of fiber components used in QKD systems at shorter wavelengths so as to identify and mitigate vulnerabilities exposed by the attack. In particular, the 400-800 nm spectral range has not been received a proper attention yet. In this paper, our goal is to fill the gap.

Note that, according to Ref. [46], successful implementation of the IPA requires low intensities starting from 3 nW. A comparison between these intensities and the maximal intensity permissible for insertion into a fiber without causing damage, which is typically around 9 W (this value is applicable to quartz single mode fibers without power damage level doping commonly used in fiber communications and may vary among manufacturers) leads to the conclusion that attenuation needed for passive defence against IPA for single pass through optical elements can roughly be estimated at about 100 dB. Thus, in order to assess the feasibility of the attack, it is necessary to measure and analyze insertion losses of individual optical elements on the side of Alice. To this end, we study the insertion losses of different optical elements in the 400–800 nm spectral range, demonstrate the existence of potential vulnerabilities and suggest potential countermeasures. The paper is organized as follows.

In Sec. II we describe our experimental technique employed to measure spectra of insertion losses of optical elements at wavelengths ranged from 400 nm to 800 nm. The experimental data for insertion losses measured for a variety of optical attenuators, wave-division multiplexing (WDM) and isolating components are presented in Sec. III. Security issues related to considered effect and proposed countermeasures are discussed in Sec. IV. Fi-

nally, in Sec. V, we discuss and summarize our results.

II. EXPERIMENTAL SETUP AND METHOD

Figure 1 shows the optical scheme of our experimental setup used to measure the insertion losses of optical elements in the visible range. In this scheme, a broadband plasma light source (XWS65, ISTEQ) indicated as the broadband light source (BLS) is utilized to produce light with wavelengths ranged from 250 nm up to 2500 nm. Referring to Fig. 1, the radiation from this source is directed into a single-mode fiber (OF) passing through a set of lenses (L), filters (F) and the objective (O) which is positioned on a three-axis stage to meet coupling and spectrum requirements. After the fiber, the focused light propagates through either a fiber or a fiber with the optical elements under test and is measured by the spectrometer (USB4000-UV-VIS-ES, Ocean Optics) with the 1.5 nm resolution.

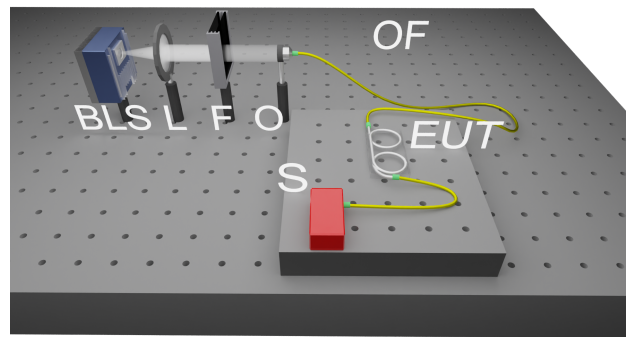


Figure 1. Optical scheme for insertion losses measurements in the visible range. BLS is broadband light source, L is lens, F is set of filters, O is objective, OF is single mode optical fiber, EUT is element under test, S is spectrometer

An important point is that the spectrometer is equipped with its own multimode fiber with an SMA905 connector. So, in order to align the single-mode and multimode fibers, we have used the FC-SMA905 connector.

Due to variations in efficiency of coupling to the single-mode fiber, losses due to absorption by the filters and technical restrictions imposed by the spectrometer, the measured spectrum of the broadband light source (BLS) was narrowed to the 400-800 nm range. Insertion losses of the optical element under test were calculated as follows:

$$\alpha_{dB}(\lambda) = -10 \log_{10} [P_{mes}(\lambda) / (P_{ref}(\lambda) T_f(\lambda))], \quad (1)$$

where the powers $P_{ref}(\lambda)$ and $P_{mes}(\lambda)$ are measured at wavelength λ without and with the tested optical element, respectively; $T_f(\lambda)$ is the transmission of the set of filters. Note that, in our experiments, the neutral filters were used to extend the dynamic range of measurements. For each element, we have performed ten measurements and the experimental results were averaged

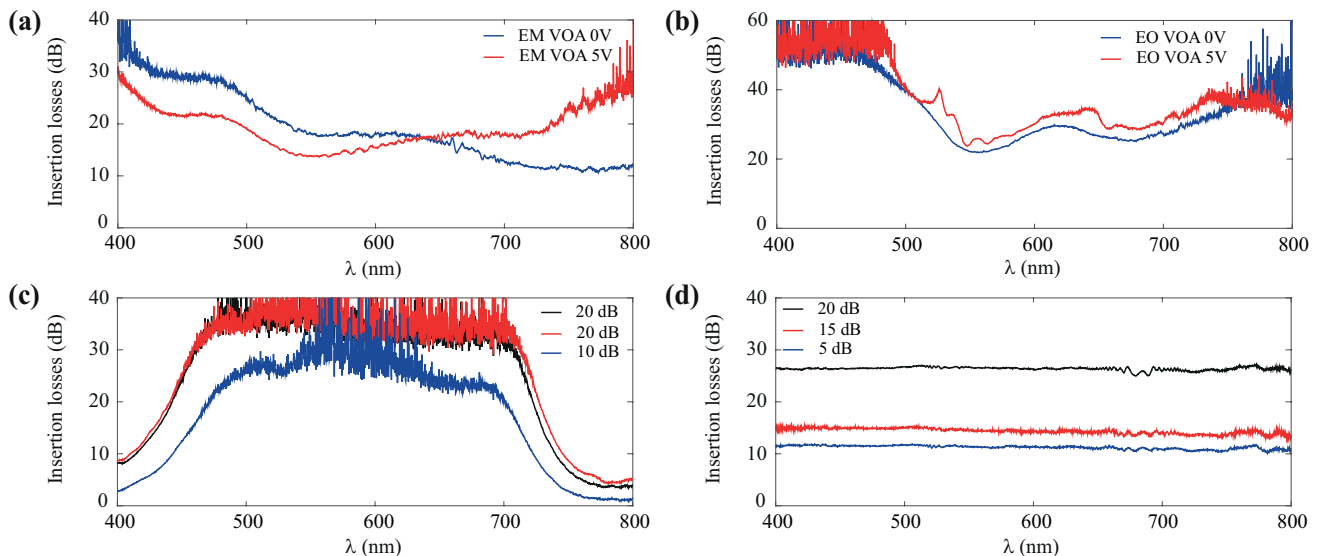


Figure 2. Insertion losses measured in the 400-800 nm range for (a) electro-mechanical and (b) electro-optical variable optical attenuators (blue and red solid lines indicate the zero-voltage curve and the case where the applied voltage is 5 V, respectively); (d) absorption based fixed attenuators (the curves for the first 20 dB FOA, second 20 dB FOA and 10 dB FOA are indicated by black, red, and blue solid lines, respectively); (c) scattering based fixed attenuators principles (the curves for 20 dB FOA, 15 dB FOA and 5 dB FOA are indicated by black, red, and blue solid lines, respectively).

(details on the error estimation procedure can be found in Appendix B of Ref. [37]). In what follows, we concentrate on the optical elements that are usually placed on the sender's side between the output of the phase and amplitude modulators and the entrance of the quantum channel.

III. EXPERIMENTAL RESULTS

A. Optical attenuators

In this section, we present the results for two variable optical attenuators (VOAs) that differ in the mode of operation, along with six different fixed optical attenuators (FOAs).

In QKD systems, optical attenuators (OA) are typically employed to reduce the intensity of laser pulses to the single photon level. Additionally, OAs are of importance in reducing the probability of wavelength-dependent attacks successful realization. Consequently, there is a requirement to avoid pronounced variations of spectral insertion loss properties of OAs across a broad wavelengths range.

In QKD systems, the insertion losses of VOAs are typically adjusted by applying voltage. This implies that during the key distribution process, the attenuation value can be tuned in the range between the maximum and minimum insertion losses. To address this variability, we have evaluated the maximal and minimal insertion losses settings for one electro-mechanical (EM) and one electro-optical (EO) model of VOA. According to the manufac-

turer datasheets, at the wavelength $\lambda = 1550$ nm, the minimal values of insertion losses without power (the field free regime without applied voltage) are 0.77 dB and 0.80 dB for EO VOA and EM VOA, respectively. When the applied voltage is 5 V, the corresponding measured values of insertion losses for EO VOA and EM VOA are 36.0 dB and 43.4 dB.

Figures 2(a) and (b) present wavelength dependencies of insertion losses measured in the 400-800 nm range for EM VOA and EO VOA at two values of applied voltage: 0 V and 5 V.

In the zero-voltage case, it turned out that the measured insertion losses are higher than the values reported in the datasheet. For EM VOA and EO VOA, the minimal losses 10.7 dB and 21.8 dB are reached at the wavelengths 761 nm and 557 nm, respectively.

Referring to Figs. 2(a) and (b), when the applied voltage is 5 V (blue lines), the losses are shown to vary in the range between 13.7 dB and 30 dB for EM VOA, whereas, for EO VOA, they are ranged from 23.7 dB to 50 dB. Note that these maximum values of losses are approximate, as they correspond to the noise level of our experimental setup and depend on the number of neutral filters.

Insertion losses measured in relation to the wavelength for six FOAs are shown in Figs. 2(c) and (d). For three absorption based FOAs (see Figs. 2(c)), according to the values reported by the manufacturers, the insertion losses of one FOA is 10 dB, whereas the losses for the other two FOAs are the same and equal to 20 dB. For the scattering based FOAs (see Figs. 2(d)), there are three different reported values of losses at the operating wavelength ($\lambda = 1550$ nm): 5 dB, 15 dB and 20 dB. Our experimen-

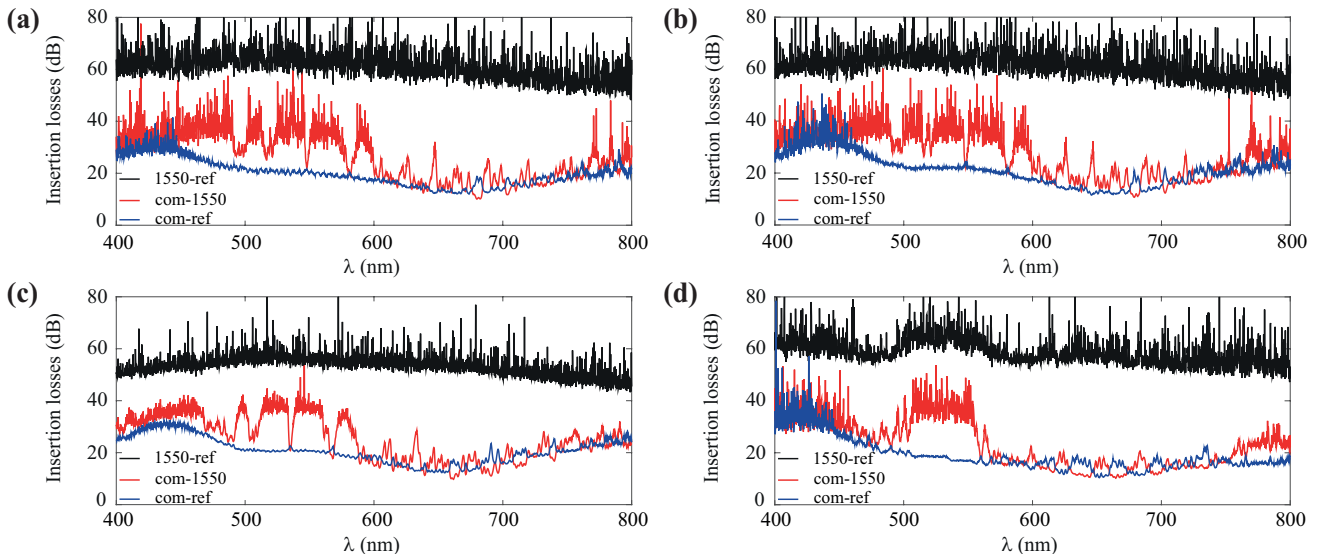


Figure 3. Insertion losses measured in the 400-800 nm range for (a) CWDM1; (b) CWDM2; (c) CWDM3 and (d) DWDM (black, blue, and red solid lines indicate insertion losses measured for light propagating along three different directions: from the ref-port to the 1550-port, from the com-port to the ref-port and from the com-port to the 1550-port, respectively)

tal results are in good agreement with these values.

The insertion losses of the absorption based FOAs measured in the 400-800 nm range are shown in Fig. 2(c). It can be seen that, for each FOA, there are two transmittance windows where the insertion losses are noticeably lower than the value at the operating wavelength indicated in the legend. The window ranged between 400 nm and 430 nm is located in the vicinity of local minima for the two 20 dB attenuators with $\alpha_{dB} \approx 8.1$ and $\alpha_{dB} \approx 8.6$ at the wavelength 405 nm (for the 10 dB attenuator, the corresponding value is $\alpha_{dB} \approx 2.7$) Similarly, the other window in the 750-800 nm wavelengths range is close to the local minima at $\lambda \approx 780$ nm with the insertion losses estimated at $\alpha_{dB} \approx 3.4$ and $\alpha_{dB} \approx 4.3$ and $\alpha_{dB} \approx 0.9$.

Figure 2(d) shows the wavelength dependencies of the insertion losses measured for the scattering based FOAs. It is seen that, for the 20 dB attenuator, the insertion losses insignificantly change with wavelength, varying from 27 dB to 25 dB. A similar conclusion applies to the 15 dB (5 dB) attenuator, where variations are between 15.6 dB (11.2 dB) and 13 dB (10.8 dB).

B. Wavelength-division multiplexing components

In QKD systems, wavelength-division multiplexing (WDM) components can be used as countermeasures by suppressing radiation with wavelengths outside the range utilized by the communication channel between Alice and Bob. In the simplest case, the key elements of the internal design of a fiber WDM component are thin films deposited on a substrate. Ideally, at the working wavelength, light will enter the common port (the com-port) and, after passing through the thin films and the sub-

strate, will propagate to the corresponding port of the operating wavelengths grid. Other wavelengths are directed to the reflecting port (the ref-port). This port might be connected with a watchdog detector that monitor Eve's probing pulses. The latter assumes that the sensitivity range of the watchdog detector is broad enough to cover wavelengths of potential attacks.

In practice, there are a number of factors limiting the efficiency of the WDM-components. These include the substrate transmittance as well as the number, ordering, and the thicknesses of the thin films. Differences between the perfectly designed mode of operation and its practical implementation may lead to side channels available to the eavesdropper. In our previous study [37], the WDM-components are found to have the transmittance windows outside the telecom range, in agreement with the theoretical calculations reported in [47].

Similar to Ref. [37], we consider both coarse WDM (CWDM) and dense WDM (DWDM) components. Specifically, insertion losses in the 400-800 nm range are measured for the four filters: three CWDM-components from the same manufacturer where two of them belong to the same production batch (CWDM1 and CWDM2) and one DWDM-component. The results are shown in Fig. 3.

In addition to the com-port and the ref-port, the WDM components have the 1550-port corresponding to the operating wavelength $\lambda = 1550$ nm. Referring to Figure 3, when the probing light propagates from the com-port to the 1550-port, each WDM-component reveals the ranges of wavelengths where the insertion losses are within the interval between 10 dB and 20 dB. Minimal values of insertion losses are presented in Table I. Note that, for the WDM-components under consideration, the losses in

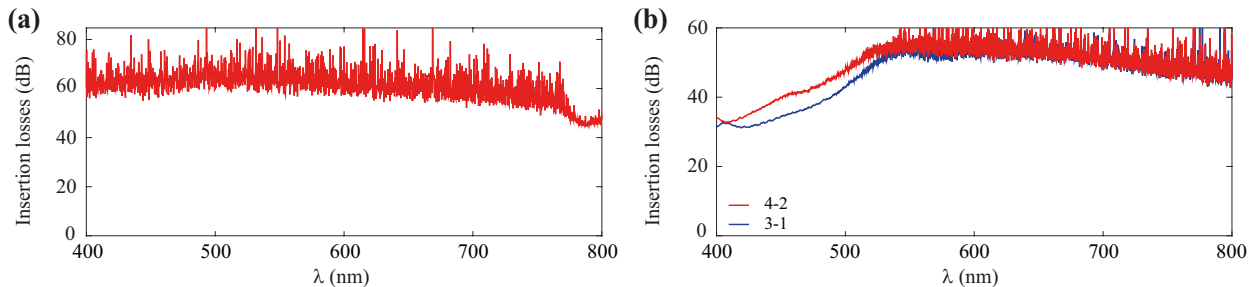


Figure 4. Insertion losses measured for (a) the dual stage isolator with light propagating from the output port to the input port; (b) the circulator (blue (red) solid lines represent insertion losses measured for light propagating from the third (fourth) port to the first (second) port).

the telecom range at non-working wavelengths are about 30 dB.

Component	α_{\min} (dB)	λ_{\min} (nm)
CWDM1	10.0	680
CWDM2	10.7	679
CWDM3	9.7	662
DWDM	10.3	665

Table I. Minimal insertion losses and corresponding wavelengths for WDM components.

From Fig. 3, it can be seen that, for the light propagating from the com-port to the ref-port, the insertion losses vary between 10 dB and 30 dB which is close to the values for the above discussed direction from the com-port to the 1550-port. For the case of light propagation from the 1550-port to the ref-port, it turned out that the losses are close to the noise level. Note that, when directions of light propagation are reversed, changes in insertion losses appear to be well below accuracy of measurements (the results of these measurements are omitted) and thus nonreciprocity effects have not been observed in our experiments.

C. Isolating components

Isolating elements are typically utilized to reduce reflections back into laser resonators. Similar to the WDM components, in QKD systems, these elements may serve as countermeasures against attacks.

In this section, we examine two elements: the dual stage isolator and the circulator. Since we are mainly interested in countermeasures against the IPA attack, the case of backward propagation of injected light where probing pulses travel from the output port to the input port will be our primary concern.

For the isolator, the spectrum of insertion losses is shown in Fig. 4(a). At the working (operating) wavelength (1550 nm), the measured insertion losses for light propagating in backward direction is about 65 dB.

From the curve depicted in Fig. 4(a), the values of measured insertion losses are mostly below the noise level

that can be detected in our experimental scheme (the dynamic range of our measurements is about 50 dB). But, in the 772-800 nm range with the minimal losses 44.5 dB reached at $\lambda = 784$ nm, the insertion losses appear to be lower than the above value at the operating wavelength.

Similar to isolators, in circulators, losses for light propagating from one port to another (forward direction) are low, whereas the light is nearly blocked when the direction of propagation is reversed (backward propagation). In contrast to the isolators, the circulators have several ports (in our case, the circulator has four ports) that opens up additional possibilities for applications in more complicated schemes. For a number of different reasons, in real devices, the insertion losses for light propagating in the backward direction will generally be wavelength dependent and may deviate from the value reported by manufacturers.

According to the datasheet for the circulator, at $\lambda = 1550$ nm, the insertion loss for backward direction is about 50 dB.

Insertion losses spectra measured for the cases where light propagates from the third (fourth) port to the first (second) bypassing the second (third) port are presented in Fig. 4(b). It can be seen that in the 400-506 nm range the losses are lower than the reported value at the working wavelength. Minimal value of insertion losses is 31.1 dB at 419 nm.

Owing to limitations of our experimental setup, we have not detected any noticeable transmission of light for backward propagation between adjacent (neighbouring) ports (for instance, propagation from the second port to the first port). In this case, the results are well below the noise level and bear close resemblance to the curves measured for the isolator.

IV. SECURITY ISSUES AND COUNTERMEASURES

It is evident that the visible spectrum does not permit the extraction of any additional information regarding signal states. Consequently, the visible spectrum can be considered as an auxiliary component of attacks aimed at

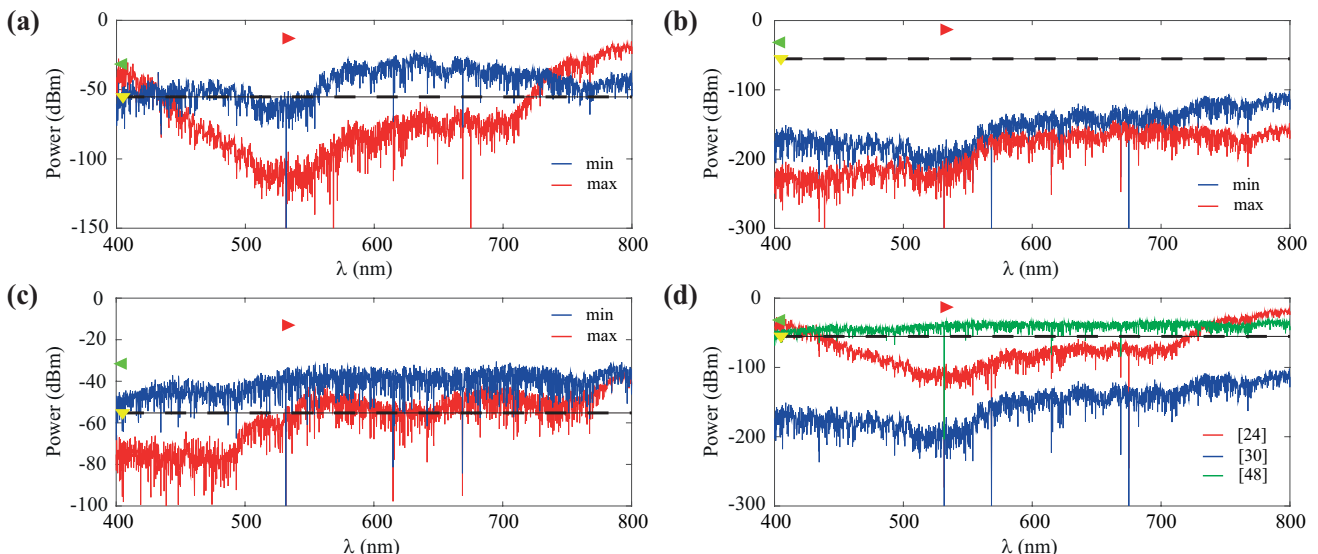


Figure 5. Estimated power that reaches the nearest investigated modulator in a system: (a) is for the scheme from [24], (b) is for the scheme from [30], (c) is for the scheme from [48]; where blue (red) solid lines represents minimal (maximal) power available to an eavesdropper. Frame (d) demonstrates the worst case of all investigated schemes (a) - (c), where blue solid line represents evaluated power for [30], red - for [24] and green - for [48], black dashed line represents conservative mean of power needed for IPA realization: yellow, red and green triangles corresponding to estimations from [46], [45] and [27] respectively

altering specific characteristics of optical elements. This includes laser damage attacks, laser seeding, and induced photorefractive attacks, among others. In the current paper, we focus our attention on the IPA attack. We analyze various QKD schemes and protocols from open sources and investigate the potential vulnerabilities that may be exploited due to this type of attack. Crucial elements influenced by IPA include various types of modulators, both phase and intensity modulators. In the following section, we consider different scenarios and their implications.

Change of PM's modulation index may be considered separately, depending on implemented optical devices. A PM can be a part of the following commonly used in the field of QKD devices:

1. PM with constant phase shift as a part of MZI scheme;
2. PM with oscillating phase shift, utilized in SCW QKD [13, 21, 28, 49];
3. PM as a part of variable attenuator;
4. PM as a part of intensity modulator.

Despite the latter classification, it is also worth mentioning that QKD protocol and utilized quantum states play essential role in security estimations. Thus, we highlight the following QKD schemes:

1. Protocols utilizing linearly dependent states (such as single-photon BB84 [50] or single-photon fraction in decoy-state protocols [12, 51, 52]), where

phase-remapping attack should be taken into consideration [53]. A number of papers are dedicated to investigate the problem for these kinds of protocols [27, 45, 46], also see Fig. 5;

2. Protocols with linearly independent set of states (coherent states with phase-coding [54–57] or SCW QKD have not been considered so far in the light of IPA auxiliary attack. Further, we draw special attention to these kinds of protocols.

First, we examine protocols utilizing coherent states and phase-coding. Changes in the modulation index lead to alterations in phase, as most QKD systems employ PM with constant phase shift as a part of MZI scheme. Thus, phase-remapping by a factor of x of is applicable:

$$\begin{aligned} & \{|\alpha_0\rangle, |\alpha_0 e^{\frac{i\pi}{N}}\rangle, |\alpha_0 e^{\frac{i2\pi}{N}}\rangle, \dots, |\alpha_0 e^{\frac{i(2N-1)\pi}{N}}\rangle\} \rightarrow \\ & \rightarrow \{|\alpha\rangle, |\alpha e^{\frac{i\pi}{N}}\rangle, |\alpha e^{\frac{i2\pi}{N}}\rangle, \dots, |\alpha e^{\frac{i(2N-1)\pi}{N}}\rangle\}, \quad (2) \end{aligned}$$

where α_0 is a complex amplitude of the coherent state, α is a complex amplitude after IPA with $|\alpha| \leq |\alpha_0|$, $2N$ is a total number of states in the set. After the IPA, the eavesdropper can apply additional commonly used attack, e.g. unambiguous state discrimination (USD) attack. The attack is characterized by the USD probability $P_U(\alpha, x)$ for a given set of states. It can be found by estimation of minimal eigenvalue of Gram matrix G , as in [58, 59]. Unfortunately, after the IPA Gram matrix loses essential properties, it no longer can be expressed as $G_{ij} \rightarrow G_{i-j}$ and becomes only symmetrical one. So an analytical result cannot be obtained for an arbitrary

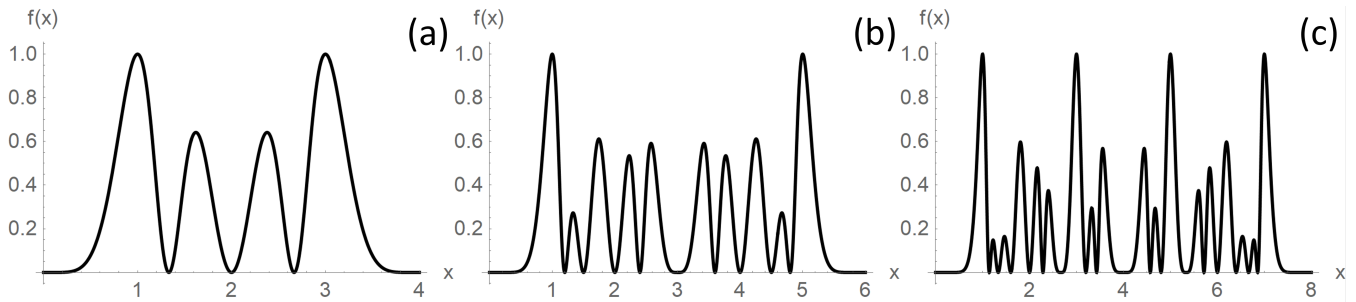


Figure 6. Dependencies $f(x)$ demonstrate decrease of unambiguous state discrimination probability in case of phase-remapping according to expression (2) for: (a) $N = 2$, (b) $N = 3$, (c) $N = 4$

number of states. However, a few analytical observations can be made. We have found that the probability can be expressed as $P_U(\alpha, x) = P_U(\alpha, 1) \cdot f(x)$ with $0 \leq f(x) \leq 1$, where $P_U(\alpha, 1)$ is USD probability. For $N = 1$, i.e. in case of just two states as in B92,

$$P_U(\alpha, x) = 1 - e^{-|\alpha|^2(1-\cos(\pi x))} \quad (3)$$

and

$$f(x) = \frac{1 - e^{-|\alpha|^2(1-\cos(\pi x))}}{1 - e^{-2|\alpha|^2}}. \quad (4)$$

Expressions for $f(x)$ in case of $N = 2$, $N = 3$ and $N = 4$ are bulky, so we demonstrate dependencies of $f(x)$ in Fig. 6. Also note, that

$$P_U(\alpha, 1) \approx \frac{2N(|\alpha|^2)^{2N-1}}{(2N-1)!}. \quad (5)$$

The overlaps of the states after the IPA only increase, so it cannot provide any significant advantage to an eavesdropper.

As for SCW QKD setup, IPA here plays the same role as attacking an IM or a VOA based on a PM in protocols with coherent states and phase-coding, since total power of sidebands is proportional to modulation index m (more precisely to $1 - J_0^2(m) \approx \frac{m^2}{2}$, where approximation is valid for small values of m and $J_0(m)$ is Bessel function of the first kind). And the latter can be increased by utilizing the IPA with a recovery, as in [45], where legitimate parties recalibrate their setups after IPA.

Countermeasure to this attack can be as follows. Before a connection of sender's setup to an optical fiber link, it's voltage, applied to the modulator, should be locked by either hardware or software (or both) and receiver's setup should calibrate only. With the proposed approach to calibration, there is no chance that the power of prepared states will be higher than it should be – only lower. So again, if countermeasure is applied, IPA provides no advantage to an eavesdropper.

However, an alternative straightforward countermeasure can be implemented. The phenomenon of IPA requires a threshold optical power to emerge. Therefore, additional losses may be simply introduced in order

to prevent illumination of the modulator with a power higher than a threshold. To illustrate the idea, we have recreated some optical schemes [24, 30, 48] in the experiment. It was based purely on their description and was performed with optical elements available to us. We emphasize that the obtained curves in Fig. 5 are mostly for illustrative purposes and may vary depending on a particular choice of optical components. In Fig 5 estimated power that reaches the nearest modulator is shown: (a) for the scheme from [24], (b) for the scheme from [30], (c) for the scheme from [48]. We compare obtained results with conservative mean of power needed for IPA realization from [27, 45, 46].

V. DISCUSSION AND CONCLUSION

In this paper, we have studied spectra of insertion losses of various fiber optical elements such as optical attenuators (see Fig. 2), WDM and isolating components (see Figs. 3 and 4, respectively) in the visible light range with wavelengths from 400 nm to 800 nm. Both the optical elements and the spectral range are important for understanding vulnerabilities of real-world QKD systems to hacking attacks, whose efficiency being wavelength dependent may noticeably improve in the visible range. Our study is motivated by one of such attacks, known as the induced-photorefractive attack [27, 45, 46].

The optical scheme behind our experimental technique enables us to perform measurements of the insertion losses with approximately 50 dB dynamic range. It is simple to use and low-cost when compared with analogous schemes discussed, e.g., in Ref. [30]. An important point is that, by using suitably modified methods presented in Ref. [38], the proposed scheme can be improved so as to extend both the wavelength range and the dynamic range of measurements. As far as certification of QKD systems is concerned, this is a feasible and easy-to-use scheme that can be employed for characterization of optical elements insertion losses.

Our experimental data show that, OAs implemented into QKD systems as countermeasures against attacks that utilize probing pulses in the visible range require

careful considerations. For VOAs, it turned out that, at certain non-vanishing voltages, the insertion losses in the visible range are lower than the losses at the operational wavelength (see Figs. 2(a)-(b)). The results for the absorption based FOAs (see Fig. 2(c)) indicate the transmittance windows that can be exploited by the IPA attack. By contrast, the insertion losses of the scattering based FOAs (see Fig. 2(d)) do not reveal noticeable changes with wavelength. So, this type of OAs is preferable as additional countermeasure against the IPA attack.

The measured spectra of all the WDM-components (see Fig. 3) have transmittance windows where insertion losses are not high enough to prevent the IPA. It is also shown that the insertion losses for light propagating from the com-port to the ref-port are ranged between 10 dB and 30 dB. Since this direction is used for active monitoring purposes, such losses combined with low efficiency of InGaAs photodiodes in the visible range will make the monitoring ineffective. One way around this problem is to use Si-based photodiodes as the watchdog detectors against optical probing pulses in the 400-800 nm range.

From the insertion loss spectrum shown in Fig. 4(a), the dual stage isolator delivers at least 44 dB insertion losses. Presumably, such losses can be attributed to absorption of magneto-optical material used in the isolator. Similar insertion losses were measured in the circulator for the case of backward propagation of light between adjacent ports.

Insertion losses for the light passing from the third port to the first port plotted against wavelength in Fig. 4(b) show that the well-known broadband filtering scheme [60] based on a Bragg grating connected to the second port of the circulator becomes ineffective in the 400-506 nm range. Thus, it cannot be employed as a reliable tool to counter the IPA.

We summarize with the remark that the scattering based FOA characterized by nearly wavelength independent losses and utilized in combination with a couple of the isolating components will deliver at least 100 dB insertion losses, which is enough to counter successful realization of the IPA.

Security issues for various types of protocols with appropriate countermeasures if necessary were considered as well. We did not cover protocols with a set of linearly dependent states, since there are a number of papers dedicated to investigate the problem. However, we have considered protocols with a set of linearly independent states, such as coherent states with phase-coding or SCW QKD protocol. Unlike the first type of protocols, the second ones are not vulnerable to IPA followed by

phase-remapping attack. For instance, as it is shown in Fig. 6, phase remapping in this case only decrease chances of unambiguous state discrimination and also does so for a general measurement outcome probability due to increase of the overlap between states. However, IPA with recovery can be done for protocols that utilized AM or IM based on PM to control the power of prepared states or where PM itself defines it, such as in SCW QKD. Here we propose either locking of the sender's voltage, applied to the modulator, so only receiver may calibrate the parameters or introduce additional insertion losses. Estimation of an amount of additional insertion losses can be done by analyzing the power that reaches the nearest investigated modulator in a system utilizing described above technique, as it shown in Fig. 5.

ACKNOWLEDGMENTS

The study is partially funded by the Ministry of Education and Science of the Russian Federation (Passport No. 2019-0903).

Appendix A: Beamsplitters

In order to present the calculated insertion losses for the investigated schemes in Fig. 5, we additionally have measured several beamsplitters. These beamsplitters are specified for 1550 nm wavelength: 50/50 beamsplitter with three connection ports, Fig. 7(a), 50/50 beamsplitter with four connection ports, Fig. 7(b), one polarization beamsplitter with three ports, Fig. 7(c), and one 99/1 with four ports, Fig. 7(d).

To simplify the perception of the figures, only the backward propagations as the insertion losses are presented, since they have a minor difference for both the forward and the backward propagation. Here we define forward connection as the propagation of scanning light from a port with a lower number to a port with a higher number, and backward connection as its opposite, for instance, see the box in Fig. 7.

For each beamsplitter, splitting ratios differ from the one of working wavelength, with an exception for the 99/1 beamsplitter. This may be useful for an eavesdropper in the case when legitimate users have not measured insertion losses for beamsplitters within the considered range and have eventually chosen lower values. However, on the other hand, it may also be used as an additional countermeasure to attenuate injected light.

[1] V. Scarani, H. Bechmann-Pasquinucci, N. J. Cerf, M. Dušek, N. Lütkenhaus, and M. Peev, The security of practical quantum key distribution, *Rev. Mod. Phys.* **81**, 1301 (2009).

[2] N. Gisin, G. Ribordy, W. Tittel, and H. Zbinden, Quantum cryptography, *Rev. Mod. Phys.* **74**, 145 (2002).

[3] R. Renner, N. Gisin, and B. Kraus, Information-theoretic security proof for quantum-key-distribution protocols,

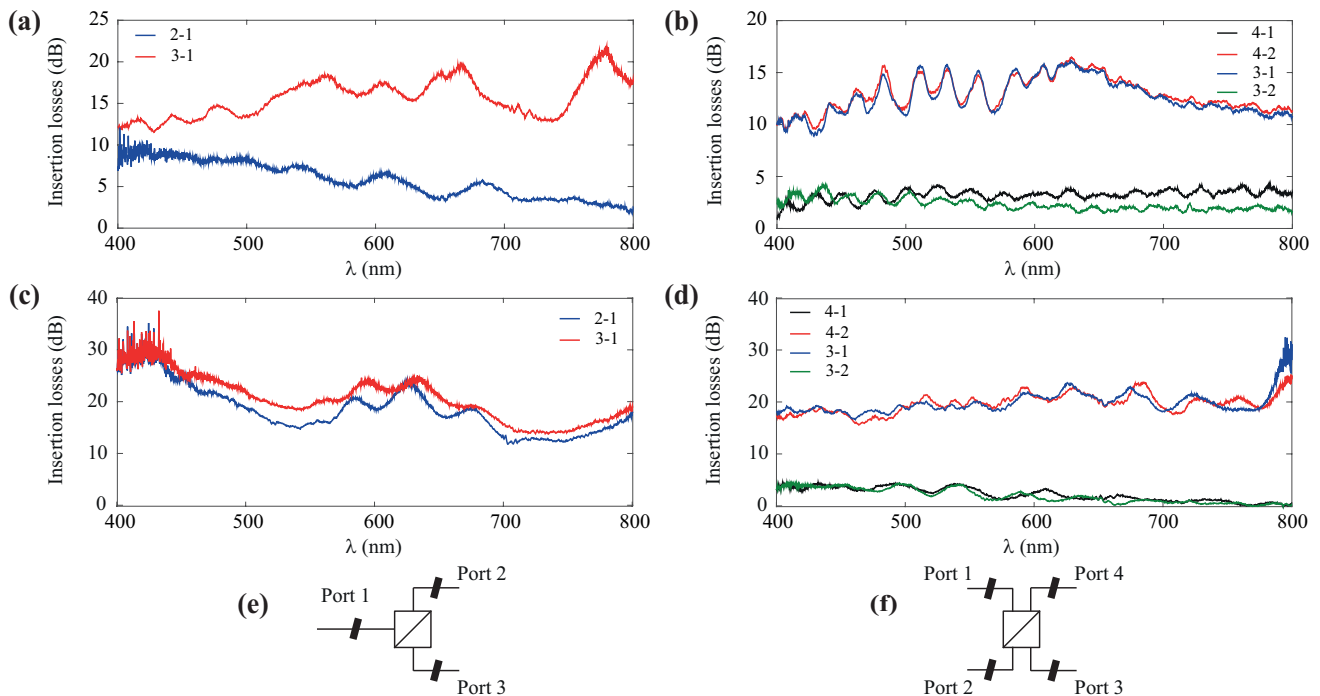


Figure 7. Insertion losses measured in the 400-800 nm range for: (a) 50/50 three-port beamsplitter, (b) 50/50 four-ports beamsplitter, (c) three-port polarization beamsplitter, (d) 99/1 four-port beamsplitter, (e) and (f) illustrate ports numeration of beamsplitters

- Physical Review A **72**, 012332 (2005).
- [4] C. Portmann and R. Renner, Cryptographic security of quantum key distribution, arXiv preprint arXiv:1409.3525 (2014).
- [5] P. W. Shor and J. Preskill, Simple proof of security of the bb84 quantum key distribution protocol, Physical review letters **85**, 441 (2000).
- [6] M. Christandl, R. Renner, and A. Ekert, A generic security proof for quantum key distribution, arXiv preprint quant-ph/0402131 (2004).
- [7] H. Inamori, N. Lütkenhaus, and D. Mayers, Unconditional security of practical quantum key distribution, The European Physical Journal D **41**, 599 (2007).
- [8] M. Ben-Or, M. Horodecki, D. W. Leung, D. Mayers, and J. Oppenheim, The universal composable security of quantum key distribution, in *Theory of Cryptography: Second Theory of Cryptography Conference, TCC 2005, Cambridge, MA, USA, February 10-12, 2005. Proceedings 2* (Springer, 2005) pp. 386–406.
- [9] A. Leverrier, R. García-Patrón, R. Renner, and N. J. Cerf, Security of continuous-variable quantum key distribution against general attacks, Physical review letters **110**, 030502 (2013).
- [10] M. Curty, T. Moroder, X. Ma, H.-K. Lo, and N. Lütkenhaus, Upper bounds for the secure key rate of the decoy-state quantum key distribution, Physical Review A **79**, 032335 (2009).
- [11] D. Gottesman, H.-K. Lo, N. Lutkenhaus, and J. Preskill, Security of quantum key distribution with imperfect devices, in *International Symposium on Information Theory, 2004. ISIT 2004. Proceedings.* (IEEE, 2004) p. 136.
- [12] H.-K. Lo, X. Ma, and K. Chen, Decoy state quantum key distribution, Physical review letters **94**, 230504 (2005).
- [13] A. Gaidash, G. Miroshnichenko, and A. Kozubov, Sub-carrier wave quantum key distribution with leaky and flawed devices, JOSA B **39**, 577 (2022).
- [14] C.-h. F. Fung, K. Tamaki, B. Qi, H.-K. Lo, and X. Ma, Security proof of quantum key distribution with detection efficiency mismatch, arXiv preprint arXiv:0802.3788 (2008).
- [15] Y. Zhang, P. J. Coles, A. Winick, J. Lin, and N. Lütkenhaus, Security proof of practical quantum key distribution with detection-efficiency mismatch, Physical Review Research **3**, 013076 (2021).
- [16] M. Bochkov and A. Trushechkin, Security of quantum key distribution with detection-efficiency mismatch in the single-photon case: Tight bounds, Physical Review A **99**, 032308 (2019).
- [17] U. Vazirani and T. Vidick, Fully device independent quantum key distribution, Communications of the ACM **62**, 133 (2019).
- [18] V. Zapatero, T. van Leent, R. Arnon-Friedman, W.-Z. Liu, Q. Zhang, H. Weinfurter, and M. Curty, Advances in device-independent quantum key distribution, npj quantum information **9**, 10 (2023).
- [19] R. Arnon-Friedman, F. Dupuis, O. Fawzi, R. Renner, and T. Vidick, Practical device-independent quantum cryptography via entropy accumulation, Nature communications **9**, 459 (2018).
- [20] R. Arnon-Friedman, R. Renner, and T. Vidick, Simple and tight device-independent security proofs, SIAM Journal on Computing **48**, 181 (2019).
- [21] V. Chistiakov, A. Kozubov, A. Gaidash, A. Gleim, and G. Miroshnichenko, Feasibility of twin-field quantum key

- distribution based on multi-mode coherent phase-coded states, *Optics Express* **27**, 36551 (2019).
- [22] H.-K. Lo, M. Curty, and B. Qi, Measurement-device-independent quantum key distribution, *Physical review letters* **108**, 130503 (2012).
- [23] S. L. Braunstein and S. Pirandola, Side-channel-free quantum key distribution, *Physical review letters* **108**, 130502 (2012).
- [24] M. Lucamarini, I. Choi, M. B. Ward, J. F. Dynes, Z. Yuan, and A. J. Shields, Practical security bounds against the trojan-horse attack in quantum key distribution, *Physical Review X* **5**, 031030 (2015).
- [25] S. Pirandola, R. Laurenza, C. Ottaviani, and L. Banchi, Fundamental limits of repeaterless quantum communications, *Nature communications* **8**, 1 (2017).
- [26] A. Acín, N. Brunner, N. Gisin, S. Massar, S. Pironio, and V. Scarani, Device-independent security of quantum cryptography against collective attacks, *Phys. Rev. Lett.* **98**, 230501 (2007).
- [27] F.-Y. Lu, P. Ye, Z.-H. Wang, S. Wang, Z.-Q. Yin, R. Wang, X.-J. Huang, W. Chen, D.-Y. He, G.-J. Fan-Yuan, *et al.*, Hacking measurement-device-independent quantum key distribution, *Optica* **10**, 520 (2023).
- [28] S. Sajeed, P. Chaiwongkhot, A. Huang, H. Qin, V. Egorov, A. Kozubov, A. Gaidash, V. Chistiakov, A. Vasiliev, A. Gleim, *et al.*, An approach for security evaluation and certification of a complete quantum communication system, *Scientific Reports* **11**, 5110 (2021).
- [29] S. Sun and A. Huang, A review of security evaluation of practical quantum key distribution system, *Entropy* **24**, 260 (2022).
- [30] V. Makarov, A. Abrikosov, P. Chaiwongkhot, A. K. Fedorov, A. Huang, E. Kiktenko, M. Petrov, A. Ponosova, D. Ruzhitskaya, A. Tayduganov, *et al.*, Preparing a commercial quantum key distribution system for certification against implementation loopholes, arXiv preprint arXiv:2310.20107 (2023).
- [31] A. Vakhitov, V. Makarov, and D. R. Hjelm, Large pulse attack as a method of conventional optical eavesdropping in quantum cryptography, *Journal of modern optics* **48**, 2023 (2001).
- [32] N. Gisin, S. Fasel, B. Kraus, H. Zbinden, and G. Ribordy, Trojan-horse attacks on quantum-key-distribution systems, *Physical Review A* **73**, 022320 (2006).
- [33] V. Makarov, Controlling passively quenched single photon detectors by bright light, *New Journal of Physics* **11**, 065003 (2009).
- [34] V. Chistiakov, A. Huang, V. Egorov, and V. Makarov, Controlling single-photon detector id210 with bright light, *Optics express* **27**, 32253 (2019).
- [35] B. Gao, Z. Wu, W. Shi, Y. Liu, D. Wang, C. Yu, A. Huang, and J. Wu, Ability of strong-pulse illumination to hack self-differencing avalanche photodiode detectors in a high-speed quantum-key-distribution system, *Physical Review A* **106**, 033713 (2022).
- [36] A. Borisova, B. Garmaev, I. Bobrov, S. Negodyaev, and I. Sinil'shchikov, Risk analysis of countermeasures against the trojan-horse attacks on quantum key distribution systems in 1260–1650 nm spectral range, *Optics and Spectroscopy* **128**, 1892 (2020).
- [37] B. Nasedkin, F. Kiselev, I. Filipov, D. Tolochko, A. Ismagilov, V. Chistiakov, A. Gaidash, A. Tsyppkin, A. Kozubov, and V. Egorov, Loopholes in the 1500–2100-nm range for quantum-key-distribution components: Prospects for Trojan-horse attacks, *Physical Review Applied* **20**, 014038 (2023).
- [38] I. S. Sushchev, D. M. Guzairova, A. N. Klimov, D. A. Dvoretzkiy, S. A. Bogdanov, K. D. Bondar, and A. P. Naumenko, Practical security analysis against the Trojan-horse attacks on fiber-based phase-coding QKD system in the wide spectral range, in *Emerging Imaging and Sensing Technologies for Security and Defence VI*, Vol. 11868 (SPIE, 2021) pp. 57–63.
- [39] N. Jain, B. Stiller, I. Khan, V. Makarov, C. Marquardt, and G. Leuchs, Risk analysis of Trojan-horse attacks on practical quantum key distribution systems, *IEEE Journal of Selected Topics in Quantum Electronics* **21**, 168 (2014).
- [40] B. Nasedkin, I. Filipov, A. Ismagilov, V. Chistiakov, F. Kiselev, A. Tsyppkin, and V. Egorov, Analyzing transmission spectra of fiber-optic elements in the near ir range to improve the security of quantum key distribution systems, *Bulletin of the Russian Academy of Sciences: Physics* **86**, 1164 (2022).
- [41] S. Alferov, K. Bugai, and I. Pargachev, Study of the vulnerability of neutral optical filters used in quantum key distribution systems against laser damage attack, *JETP Letters* **116**, 123 (2022).
- [42] A. Huang, R. Li, V. Egorov, S. Tchouragoulov, K. Kumar, and V. Makarov, Laser-damage attack against optical attenuators in quantum key distribution, *Physical Review Applied* **13**, 034017 (2020).
- [43] A. Ponosova, D. Ruzhitskaya, P. Chaiwongkhot, V. Egorov, V. Makarov, and A. Huang, Protecting fiber-optic quantum key distribution sources against light-injection attacks, *PRX Quantum* **3**, 040307 (2022).
- [44] P. Chaiwongkhot, J. Zhong, A. Huang, H. Qin, S.-c. Shi, and V. Makarov, Faking photon number on a transition-edge sensor, *EPJ Quantum Technology* **9**, 23 (2022).
- [45] L. Han, Y. Li, H. Tan, W. Zhang, W. Cai, J. Yin, J. Ren, F. Xu, S. Liao, and C. Peng, Effect of light injection on the security of practical quantum key distribution, *Physical Review Applied* **20**, 044013 (2023).
- [46] P. Ye, W. Chen, G.-W. Zhang, F.-Y. Lu, F.-X. Wang, G.-Z. Huang, S. Wang, D.-Y. He, Z.-Q. Yin, G.-C. Guo, *et al.*, Induced-photorefractive attack against quantum key distribution, *Physical Review Applied* **19**, 054052 (2023).
- [47] P.-f. Gu and Z.-r. Zheng, Design of non-polarizing thin film edge filters, *Journal of Zhejiang University-SCIENCE A* **7**, 1037 (2006).
- [48] A. A. Hajomer, I. Derkach, N. Jain, H.-M. Chin, U. L. Andersen, and T. Gehring, Long-distance continuous-variable quantum key distribution over 100-km fiber with local local oscillator, *Science Advances* **10**, eadi9474 (2024).
- [49] G. Miroschnichenko, A. Kozubov, A. Gaidash, A. Gleim, and D. Horoshko, Security of subcarrier wave quantum key distribution against the collective beam-splitting attack, *Optics express* **26**, 11292 (2018).
- [50] C. H. Bennett and G. Brassard, Quantum cryptography: Public key distribution and coin tossing, *Theoretical computer science* **560**, 7 (2014).
- [51] X. Ma, B. Qi, Y. Zhao, and H.-K. Lo, Practical decoy state for quantum key distribution, *Physical Review A—Atomic, Molecular, and Optical Physics* **72**, 012326 (2005).
- [52] X.-B. Wang, Beating the photon-number-splitting attack

- in practical quantum cryptography, *Physical review letters* **94**, 230503 (2005).
- [53] C.-H. F. Fung, B. Qi, K. Tamaki, and H.-K. Lo, Phase-remapping attack in practical quantum-key-distribution systems, *Physical Review A—Atomic, Molecular, and Optical Physics* **75**, 032314 (2007).
- [54] C. H. Bennett, Quantum cryptography using any two nonorthogonal states, *Physical review letters* **68**, 3121 (1992).
- [55] H.-K. Lo and J. Preskill, Security of quantum key distribution using weak coherent states with nonrandom phases, arXiv preprint quant-ph/0610203 (2006).
- [56] C. H. Bennett, F. Bessette, G. Brassard, L. Salvail, and J. Smolin, Experimental quantum cryptography, *Journal of cryptology* **5**, 3 (1992).
- [57] C. Gobby, a. Yuan, and A. Shields, Quantum key distribution over 122 km of standard telecom fiber, *Applied Physics Letters* **84**, 3762 (2004).
- [58] A. Kozubov, A. Gaidash, and G. Miroshnichenko, Quantum control attack: Towards joint estimation of protocol and hardware loopholes, *Physical Review A* **104**, 022603 (2021).
- [59] A. Gaidash, A. Kozubov, and G. Miroshnichenko, Methods of decreasing the unambiguous state discrimination probability for subcarrier wave quantum key distribution systems, *JOSA B* **36**, B16 (2019).
- [60] I. Riant, Fiber bragg gratings for optical telecommunications, *Comptes Rendus Physique* **4**, 41 (2003).